THE GREAT WORLD OF NANOTECHNOLOGY

Marcos Augusto de Lima Nobre

(Organizador)

VOL II

EDITORA ARTEMIS
2021

THE GREAT WORLD OF NANOTECHNOLOGY

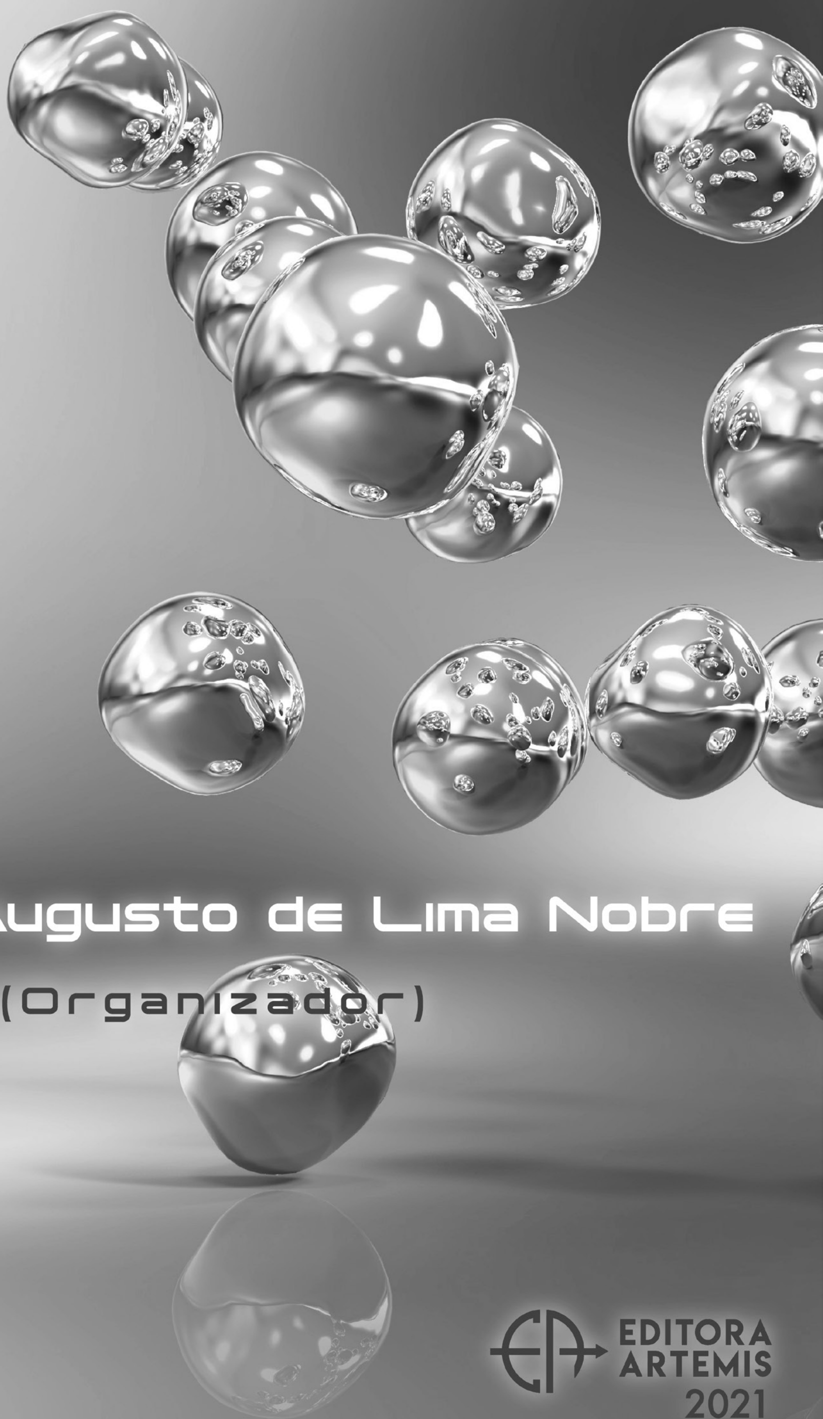

Marcos Augusto de Lima Nobre

(Organizador)

VOL II

EDITORA ARTEMIS

2021

Editora Chefe Profª Drª Antonella Carvalho de Oliveira
Editora Executiva M.ª Viviane Carvalho Mocellin
Direção de Arte M.ª Bruna Bejarano
Diagramação Elisangela Abreu
Organizadoras Prof. Dr. Marcos Augusto de Lima Nobre
Imagem da Capa Kateryna Kon
Bibliotecário Maurício Amormino Júnior – CRB6/2422

Editora Artemis
Curitiba-PR Brasil
www.editoraartemis.com.br
e-mail:publicar@editoraartemis.com.br

Dados Internacionais de Catalogação na Publicação (CIP)
(eDOC BRASIL, Belo Horizonte/MG)

G786 The great world of nanotechnology [livro eletrônico] : vol. II / Organizador Marcos Augusto de Lima Nobre. – Curitiba, PR: Artemis, 2021.

Formato: PDF
Requisitos de sistema: Adobe Acrobat Reader
Modo de acesso: World Wide Web
Inclui bibliografia
Edição bilíngue
ISBN 978-65-87396-36-1
DOI 10.37572/EdArt_300621361

1. Nanociência. 2. Nanotecnologia. I. Nobre, Marcos Augusto Lima.

CDD 620.5

Elaborado por Maurício Amormino Júnior – CRB6/2422

EDITORA ARTEMIS
2021

Editora Artemis
Curitiba-PR Brasil
www.editoraartemis.com.br
e-mail:publicar@editoraartemis.com.br

PREFACE

The insertion of new and enhanced materials based on materials belonging to the Nano scale in the day-by-day has growth up in a silent way. In part, a number of works in the nanotechnology stemming of theoretical research using Density Functional Theory (DFT) and sophisticated simulation methods; another part is associated to the protected technologies associated to the military and patented nanomaterial and its process. In this sense, open access to recent aspects on the nanostructures application and properties can be reached in this book. Here, an interesting set of chapters gives opportunity of access texts that reach process and processing of nanostructures, applications of nanotechnology, advanced techniques to theoretical development. A broad set of nanostructures are here covered such as, nanocrystal, superficial nanograins, inner microstructures with nanograins, nanoaggregates, nanoshells, nanotubes, nanoflowers, nanoroad, nanosheets, Also, reveals new investigations areas as grainboundary of nanograins in ceramics and metals. A great number of software has been used as a tool of development of Science and Technologies for nanotechnology COMSOL Multiphysics 5.2. Phenomena and properties has been investigated by recent or classical techniques of materials characterization as Localized Surface Plasmon Resonance (LSPR), X-ray photoelectron spectroscopy (XPS), Field Emission Gun Scanning Electron Microscopy (FEG-SEM) with Energy Dispersive Spectroscopy (EDS), Raman Scattering Spectroscopy (RSS), X ray diffraction (XRD), ^{57}Fe Mössbauer spectroscopy, UV-vis spectroscopy, dynamic light scattering (DLS), Atomic Force Microscopy (AFM), and Field Emission Gun Scanning Electron Microscopy (FEG-SEM). In this sense, collections of spectra from Mössbauer spectroscopy, UV-vis spectroscopy and Infrared spectroscopy can be found. As a matter of fact, some chapter’s item can be seemed as specific protocols for synthesis, preparations and measurements in the nanotechnology.

I hope you enjoy your reading.

Prof. Dr. Marcos Augusto Lima Nobre

TABLE OF CONTENTS

CHAPTER 10

NANOGRAIN BOUNDARY PHENOMENON IN CERAMIC NANOMETRIC MICROSTRUCTURE[1]

Data de aceite: 15/05/2021

Marcos Augusto Lima Nobre
São Paulo State University, School of Technology and Sciences – FCT/UNESP
Department of Physics
Presidente Prudente – SP
http://lattes.cnpq.br/7201928600704530

Silvania Lanfredi
São Paulo State University School of Technology and Sciences – FCT/UNESP
Department of Chemistry and Biochemistry
Presidente Prudente – SP
http://lattes.cnpq.br/0239752189917951

ABSTRACT: Nanograin boundary relaxation frequency phenomenon at cryogenic temperatures of $KSr_2Nb_5O_{15}$ ceramic with microstructure based on nanosized grains has been investigated. The presence of nanosized microstructure results in an increasing of "grain boundary" contribution dielectric response. A process to derive the nanograin relaxation frequency assigned to nanograins boundary from deconvolution of the Imaginary component of impedance is discussed.

KEYWORDS: Nanotechnology. Nanostructures. Nanograins. $KSr_2Nb_5O_{15}$ ceramic.

1 INTRODUCTION

Compounds based on niobium and alkali and alkaline earth metals have been considered one of the most promising ferroelectric materials. Among these compounds stands out the strontium potassium niobate, $KSr_2Nb_5O_{15}$, with tetragonal tungsten bronze, TTB-type structure. However, only in recent years that these materials have attracted attention. This fact suggests that there is a potential for the discovery of new ferroelectric materials. In addition, the development of new materials is not only relevant, well as the monitoring of the properties of these materials in nanometric scales is fundamental. This aspect is important to the design of properties and new technologies involving nanometric and/or nanostructured ceramics, multilayer capacitors, polymer-ceramic composites.

The scale effect can be considered a phenomenon that describes the appearance or disappearance of a material property due to the variation in the dimensional scale. A similar

[1] This chapter is the translation of the chapter published in the book: The great world of nanotechnology / Organizador Marcos Augusto Lima Nobre. – Curitiba, PR: Artemis, 2020, Cap. 6, p. 59.

effect, denominated particle size effect, is attributed to the intensification or reduction of a property of the material due to the dimensional variation, however this property exists regardless of the scale.

Nanoparticles, nanopowders and nanostructured materials have been used with great success to allow optical, calorimetric, mechanical, magnetic and electrical resistance properties, as a function of scale and size effects. In fact, in the nanometric scale, size effects are also relevant to structural properties.

The tetragonal tungsten bronze TTB-type structure belongs to an important class of ferroelectric materials, from a series of lead-free compounds. This TTB structure has the capacity to arrange cations of different ionic radius and different valences along their interstitial sites (Magneli, 1949).

The TTB-type structure consists of a complex matrix of octahedral distortions BO6, in order to generate cavities and/or crystallographic sites denominated A, B and C, where these correspond to the pentagonal, tetragonal and trigonal sites, respectively (Abrahams et al.,1971; Tribotte et al., 1998; Lanfredi et al. 2004).

The TTB-niobate structure can be further described by the general formula $(A1)_2(A2)_4C_4(B1)_2(B2)_8O_{30}$. A1 and A2 occupy 12-fold coordinated and 15-fold coordinated tunnels, respectively. C sites are typically vacant. (B1) and (B2) sites are resulting from two types of octahedral distortions BO6.

The TTB-type structure enables the substitution of a wide-variety of cations in the A1, A2 sites, in particular alkali and alkaline earth. Other substitutions based on the transition metal are viable in the (B1) and (B2) sites. The cations substitution in the different sites of the structure have a significant effect on its dielectric properties (Lanfredi et al., 2012).

Strontium potassium niobate has attracted particular interest for presenting several properties such as ferroelectric, dielectric, piezoelectric, high polarization (Shanming et al., 2008; Lanfredi et al. 2014), besides to have electro-optical, catalytic and photocatalytic properties (Matos et al., 2017) .

This work provides a comprehensive report on the structural thermal stability of the $KSr_2Nb_5O_{15}$ powder investigated by X-ray diffraction and the dielectric-permittivity properties at cryogenic temperatures of $KSr_2Nb_5O_{15}$ ceramic with microstructure based on nanosized grains. The correlations between thermal hysteresis of dielectric permittivity and non structural phase transitions are established.

2 SYNTHESIS OF THE NIOBATE POWDER BY THE MODIFIED POLYOL METHOD

The Modified Polyol Method (Lanfredi et al., 2012) was used in this work for the chemical synthesis of strontium and potassium niobate powders with stoichiometry

$KSr_2Nb_5O_{15}$. This method allows the synthesis of powders in areduced number of steps and the obtention of single-phase powders. The first step consists of the mixing of starting reagents followed by the pre-calcination, giving rise to the precursor powders. Then, the precursor was calcined in order to obtain single-phase and crystalline powders. The starting reagents for the powder synthesis via chemical route were nitric acid HNO_3 (99.5% Reagen), strontium carbonate $SrCO_3$ (99.0% Reagen), potassium carbonate K_2CO_3 (99.0% Reagen), ethylene glycol $HOCH_2CH_2OH$ (98.0 % Synth) and hydrated niobium oxide ($Nb_2O_5.3.28H_2O$) (CBMM-Brazil).

In a beaker was added niobium oxide to which was dripped slowly nitric acid until its dissolution. Then, strontium and potassium carbonates were added gradually, and again, drops of concentrated nitric acid were added. After dissolving all the starting salts, 100 ml of ethylene glycol was added in the mixture, which was submitted to heating at 423K.

The gradual increase in temperature caused the release of a gas of brown color, due to the decomposition of the nitric acid, similar to the reaction developed in the synthesis by the Polymeric Precursor Method, or Pechini (Pechini, 1967; Lanfredi et al., 2004).

The gas formed was the NO_2, resulting of the pyrolysis of the nitrate group in solution, according to the chemical reaction:

$$NO_3^-(aq) \underset{\Delta}{\rightarrow} NO_2(g) + \frac{1}{2}O_2(g) \quad (1)$$

After this process, a gel polymeric is obtained. Then, the gel polymeric is maintained in the beaker undergoes a primary calcination in a furnace type box. The heating cycle was carried out using two steps.

In the first step, the temperature was increased using a heating rate equal to 10 K/min from room temperature up to 423 K. At this point, the temperature was kept constant during 1 hour for eliminating low molecular mass molecules, such as water vapor and some organic groups. In the second step, maintaining the same heating rate, the temperature was increased at 573 K, being maintained during 2 hours for the partial elimination of elements not belonging to the stoichiometry of solid solutions, such as CO, CO_2 and H_2O molecules. Both pre-calcination steps were performed under an N_2 (g) atmosphere with a flow rate of 300 mL/min. After the cycle, the furnace was cooling to the natural rate.

After pre-calcination, the precursor powder was obtained in the form of black porous charcoal, which was deagglomerate in an agate mortar and then in a sieve of 325 mesh with opening of 45 μm. Then, the precursor powder exhibited a dark gray color and a fine and homogeneous aspect. The precursor powder was calcined in a furnace type box at 1423 K for 10 hours, in oxygen atmosphere with flux of 300 mL/min, and then the furnace was cooling to the natural rate.

2.1 STRUCTURAL CHARACTERIZATION OF THE $KSR_2NB_5O_{15}$ POWDER

Structural analysis of the $NaSr_2Nb_5O_{15}$ powder was carried out by X-ray diffraction (XRD), using a SHIMADZU (model XRD-6000) diffractometer with Cu-Kα radiation (λ = 1.54 Å) and a graphite monochromator. Measurements were carried out at 40kV e 30mA over an angular range of $5^o \leq 2\theta \leq 80^o$ with a scanning step of 0.02^o and a fixed counting time of 1.2s. Divergence, scattered and receiving radiation slits were 1^o, $1\,^o$ and 0.3 mm, respectively.

The $KSr_2Nb_5O_{15}$ structure was refined according to the Rietveld method using the Fullprof program FullProf (Carvajal, 2008). The parameters and variables adopted during the refinement process were the background coefficients, profile coefficients, lattice parameters, linear absorption coefficients, coordination parameters and structure factor.

The data obtained, from the structural parameters refinement, were used in the Diamond program to build the crystallographic structure of the $KSr_2Nb_5O_{15}$.

2.2 ELECTRICAL CHARACTERIZATION OF THE $KSr_2Nb_5O_{15}$ CERÂMIC

Prior to the sintering, the powder was uniaxially pressed into pellet form of 8x2 mm dimension. The green compact was sintered at 1553 K in air for 2 h at a heating rate of 2.0 K/min. Relative density equal to 97 % of the theoretical density was reached. Microstructure was characterized using scanning electron microscopy – SEM (Zeiss DSM 962).

Electric measurements were carried out by impedance spectroscopy over a complete thermal cycle. Electrodes were deposited on both faces of the sample with a platinum paste coating (TR-7905 –Tanaka). After complete solvent evaporation, the electrode/ceramic was dried at 1073 K for 30 min. Measurements were taken in the frequency range of 5 Hz to 13 MHz, with an applied potential of 500 mV using an Impedance Analyzer Alpha N High Resolution Dielectric from Novocontrol GmbH. The sample was placed in a sample holder with a two-electrode configuration. Measurements were taken from room temperature to 800 K in 50-K steps at a heating rate equal to 1.0 K/min in air. A 30-min interval was used prior to thermal stabilization before each measurement. The data were plotted using the complex plane formalism ortho-normalized, *Z' (ω) versus Z" (ω)* plot, and analyzed with Boukamp's EQUIVCRT software.

Dielectric spectroscopy characterization was performed in the frequency range of 1 kHz to 1 MHz and a temperature range of 15K to 800 K.

The complex permittivity function $\varepsilon^*(\omega)$ was derived from the impedance function, $Z^*(\omega)$:

$$Z^*(\omega) = \sum_i^n Z_i^*(\omega) = Z_1^*(\omega) + Z_2^*(\omega) + \ldots + Z_n^*(\omega) \quad (2)$$

$$Z^*(\omega) = \sum_i^n Z_i'(\omega) + j\sum_i^n Z_i''(\omega) = \sum_i^n \mathrm{Re}_i(Z) + j\sum_i^n \mathrm{Im}_i(Z) \quad (3)$$

where $Z^*(\omega)$ is an apparent response composed by the contribution of all electroactive components of the system and can be represented by Eq. (2) and (3), n is the number of electroactive component of the system. The most frequent response to $Z^*(\omega)$ is a semicircle which can be decentralized or not be. In a general way, this semicircle is an apparent response which represents a combination of two or more semicircles, as example grain and grain boundary (Lanfredi et al., 2012). Each semicircle can be fulfil observed on the impedance diagram only if the relaxation frequency that ascribes each semicircle differ at least of two orders of magnitude.

Typically, for polycrystalline ceramic systems, the impedance can be described by two electroactives contributions assigned to the grain (G) and the grain boundaries (GB). From Eq. (2) determines the impedance of the system given by Eq. (4):

$$Z^*_{CERAMIC}(\grave{u}) = Z_G^*(\omega) + Z_B^*(\omega) \quad (4)$$

From of the function transformation $\varepsilon^*_{CERAMIC}(\omega) = [j\omega\varepsilon_0\Lambda Z^*(\omega)]^{-1}$, these components of transformation relationships are given by the Eq. (5), as follows (Nobre e Lanfredi, 2000):

$$\varepsilon^*_{CERAMIC}(\omega) = \frac{1}{j\omega\varepsilon_0\Lambda Z^*(\omega)} = \begin{cases} \varepsilon'(\omega) = -\dfrac{1}{\Lambda\omega\varepsilon_0}\left(\dfrac{Z''(\omega)}{|Z^*|^2}\right) \\ \varepsilon''(\omega) = \dfrac{1}{\Lambda\omega\varepsilon_0}\left(\dfrac{Z'(\omega)}{|Z^*|^2}\right) \end{cases} \quad (5)$$

where Λ represents the geometric factor of the cell, ω represents the angular frequency ($\omega = 2\pi f$), ε_0 represents the vacuum permittivity constant (8.8542 x 10^{-12} F/m), and $|Z^*(\omega)|$ represents the module of the impedance; $\varepsilon'(\omega)$ and $\varepsilon''(\omega)$ represent both the real and imaginary component of the complex dielectric permittivity $\varepsilon^*(\omega)$, respectively.

3 STRUCTURAL ANALYSIS

The $KSr_2Nb_5O_{15}$ powder exhibited only a set of diffraction lines ascribed to the TTB-type structure. The structural parameters of $KSr_2Nb_5O_{15}$ were derived the Rietveld method. The Rietveld plot for the $KSr_2Nb_5O_{15}$ is shown in Figure 1.

Figure 1: Rietveld plot for the $KSr_2Nb_5O_{15}$ powder obtained at 1423 K for 10h.

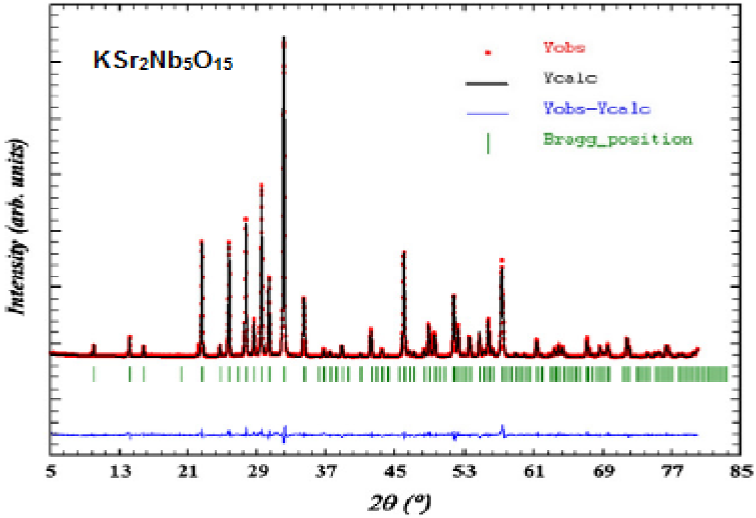

The best refinements were performed by taking into account the space groups P4bm that are compatible with the rule of existence [(*0 k l*) *k* = 2*n*], where each tetragonal site was occupied by a Sr^{2+} ion and each pentagonal site was statistically occupied by equal quantities of K^+ and Sr^{2+} ions. The trigonal site was considered vacant. two non-equivalent octahedral sites are occupied by Nb^{5+} cations called Nb (1) and Nb (2) (Lanfredi et al., 2004).

Figure 2 shows the graphic representation of the unit cell obtained for $KSr_2Nb_5O_{15}$ powder at 1423 K for 10h.

Figure 2: Tetragonal tungsten bronze structure of the $KSr_2Nb_5O_{15}$ powder obtained at 1423K for 10h.

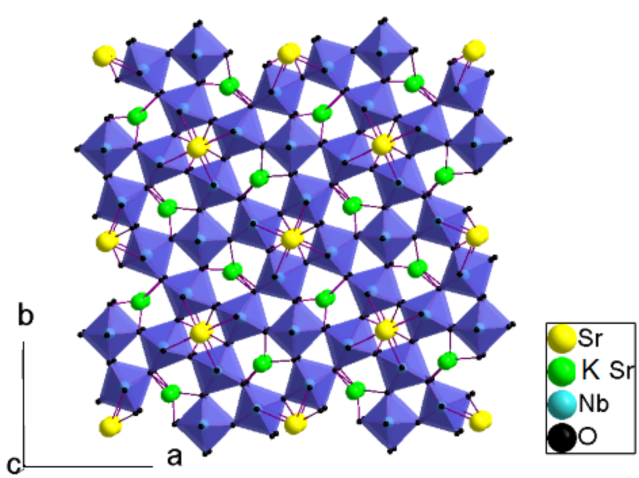

4 MICROESTRUCTURAL ANALYSIS

Figure 3 shows the scanning electron microscopy (SEM) image of the $KSr_2Nb_5O_{15}$ ceramic sintered at 1553 K for 2 h.

Figure 3: Scanning electron microscopy image of the nanostructured ceramic.

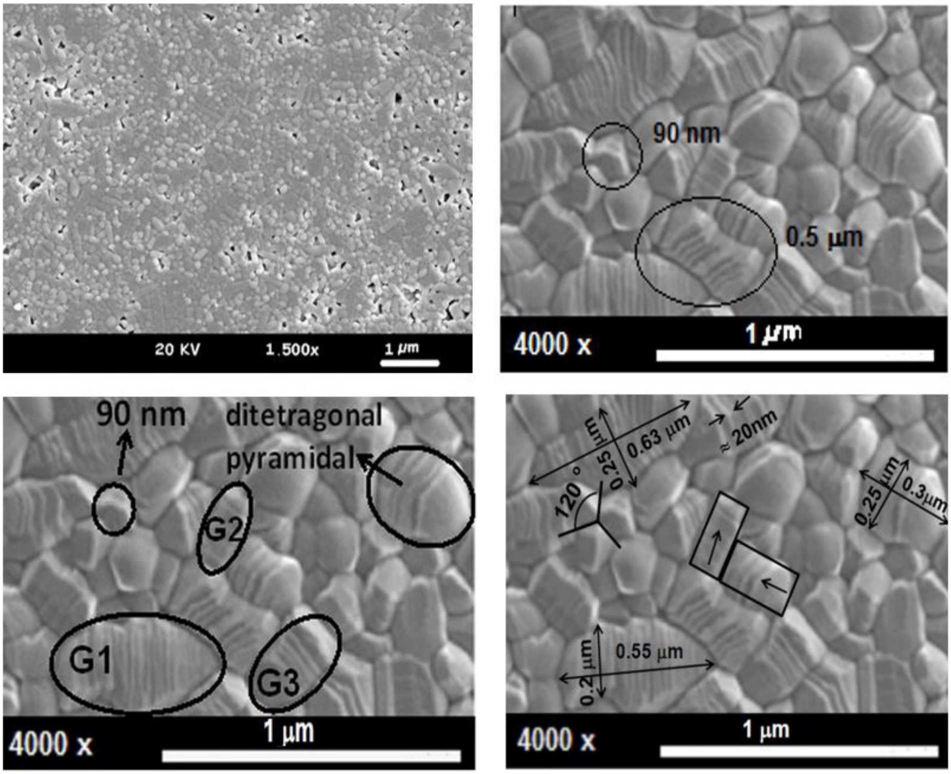

The microstructure shows few pores and nanosized grains. The inset shows an expanded region of Figure 3 that exhibits some grains with anisotropic growth because the growth rate in the *c-axis* direction [001] is faster than that in the *a-axis* direction, resulting in a growth and displacement of grains, as can be seen in G1, G2 and G3.

According to Figure 3, grains are formed by a substructure of ≈ 20 nm. The formation of theses substructures are due the displacement of grains that can be observed along of grains of size of 0.3 µm, 0.55 µm and 0.63µm of length and of 0.20 µm and 0.25 µm of wide. Such substructure seems be generated by perpendicular forces to c-axes, which leads to the cleavage phenomenon.

5 ANALYSIS OF ELECTRICAL PROPERTIES

Figure 4 shows the $KSr_2Nb_5O_{15}$ impedance diagram and theoretical adjustment attained at 600 K.

Figure 4: Impedance diagram (Z' (ω) vs Z" (ω)) and theoretical adjustment obtained at 600 K.

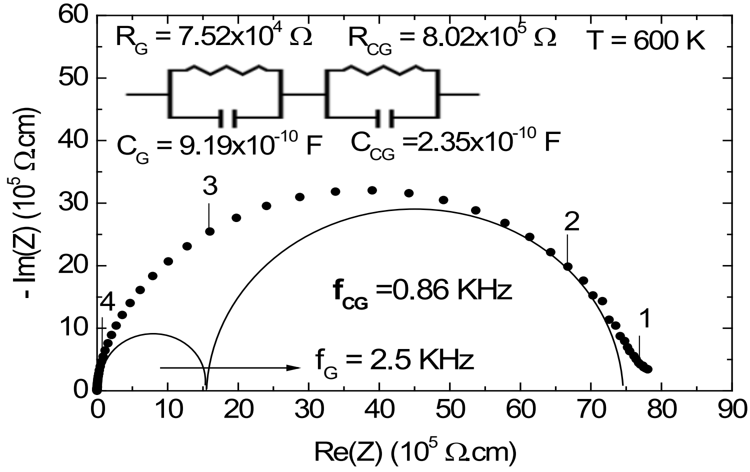

According to Figure 4, points on the plot represent the experimental data, while the continuous line represents the theoretical adjustment. The agreement between the experimental points and the theoretical curve is excellent.

The electric response is well represented by four equivalent parallel *RC* circuits in series, where *R* represents the resistance and *C* represents the capacitance.

The semicircle at low frequency (<10^3 Hz) represents the grain boundary contributions and the semicircle at high frequency (> 10^3 Hz) represents the contribution corresponding to the grain or bulk. The relaxation frequency of the grain is at around 2.5 KHz, while for the grain boundary is of 0.86 KHz. The same relaxation frequency values were obtained from adjustment of the imaginary part curve, Z" (ω), as a function of log f, as shown in Figure 5. The adjustment was performed by two Gaussian functions.

Figure 5: Z" (ω) as a function of log f adjusted by two Gaussian functions.

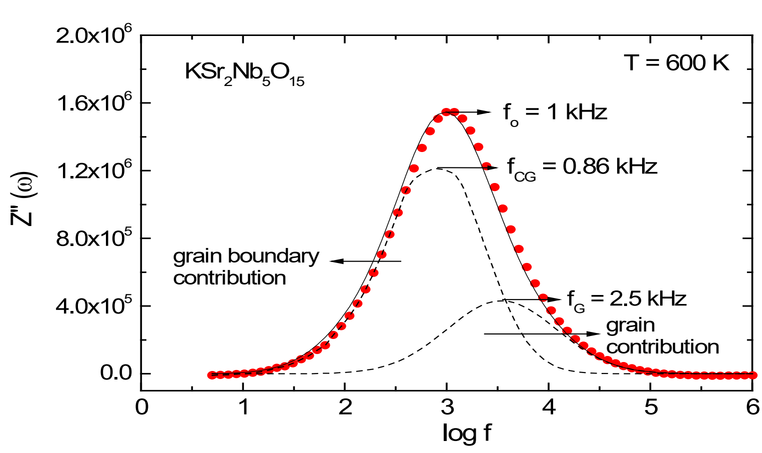

6 ANALYSIS OF DIELECTRIC PROPERTIES

Figure 6 shows the real part ε'(ω) and the imaginary part ε"(ω) of the complex dielectric permittivity $\varepsilon^*(\omega)$ as a function of temperature at several frequencies.

Figure 6: Evolution of the real (ε') part and imaginary (ε") part of the complex dielectric permittivity of $KSr_2Nb_5O_{15}$ ceramic.

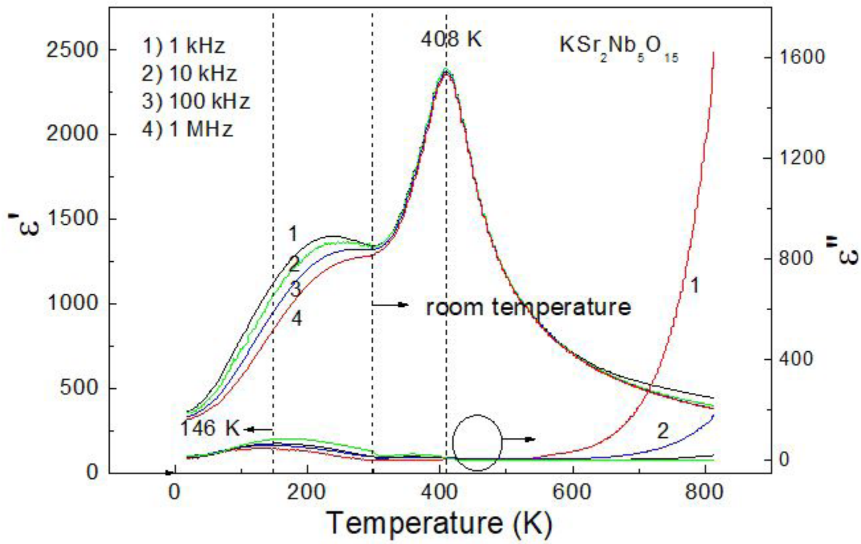

A visual inspection of curves shows two broad peaks or anomalies in both the ε' (ω) and ε"(ω) curves. Considering the peak-superposition phenomenon, an apparent peak in ε'(T) is closely centered at 255 K as a shoulder with a very broad peak, while a defined peak is positioned at 408 K. the apparent relative maximum of ε' at approximately 255 K also has been observed as function of the frequency of measurement. The dependence of a maximum value of permittivity with a frequency has been assigned to some degree of chemical and structural disorder. Therefore, the phenomenon observed at approximately 255 K as function of the frequency can be resulted of different domains in the structure. On the other hand, the peak centered at close to 408 K exhibits a sharp absolute-maximum (ε' = 2375) in the ε'(ω) *versus* T curve and has been assigned to the ferroelectric-paraelectric transition due the Curie's temperature (Belghiti al., 2002). A single peak in the ε" (ω) versus T curve of small intensity, occurring as a broader peak at approximately 146 K, is attributed to the existence of dielectric loss by conduction (Lanfredi et al., 2002).

Figure 7 shows the evolution of the real permittivity, ε', as a function of temperature, measured at 1 KHz during the heating cycle.

Figure 7: Permittivity curves as a function of temperature measured at 1 kHz.

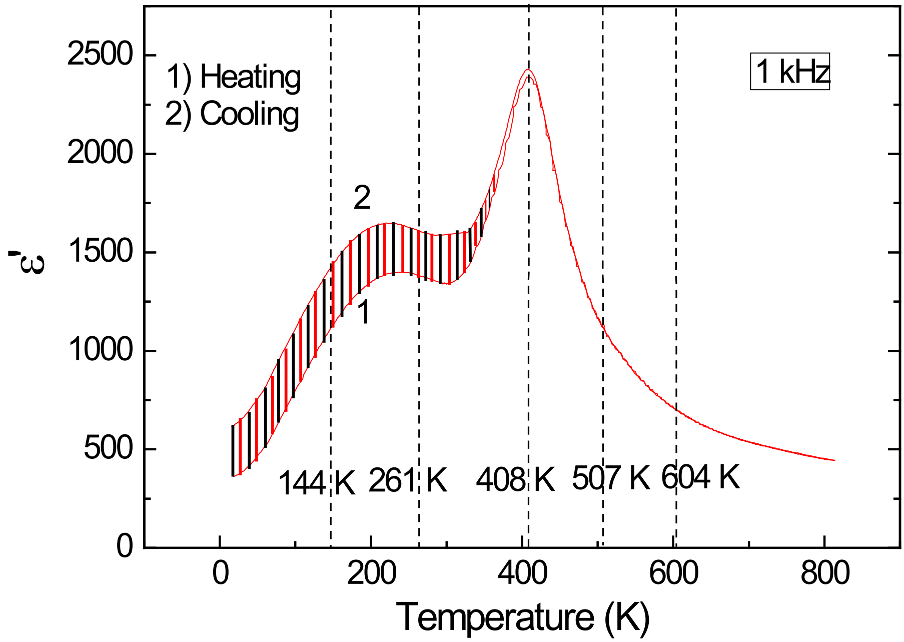

The ε' parameter exhibits a well-behavioured thermal-hysteresis at cryogenic temperatures domain, see the dashed area. Typically, mixture of phases of same stoichiometry but distinct symmetry structure gives the above mentioned hysteretical effect (Nobre e Lanfredi, 2001). A significant area of thermal hysteresis below 408 K strongly suggests that there are not a structural phase transition corroborated by the specific lattice parameter evolution and that non exhibits discontinuous or abrupt changing. Then, significant part of the phenomenon has only basis on the structural distortion. These phase transitions observed in the permittivity curves are confirmed in the permittivity inverse curve as a function of temperature, shown in Figure 8. The sequence of phase transitions can be related to the coexistence of same symmetry phases, but with a particular crystal lattice distortion. This concept is relevant, since the transitions can be structural or not. If a sufficient degree of distortion is generated, a new symmetry can emerge, otherwise the phase transition occurs, but the symmetry of the prototype is maintained, while only specific distortions are allowed, such as the distortion of the niobium off-center in the NbO_6 octahedral of the tetragonal tungsten bronze structure.

Figure 8: Permittivity inverse as a function of temperature.

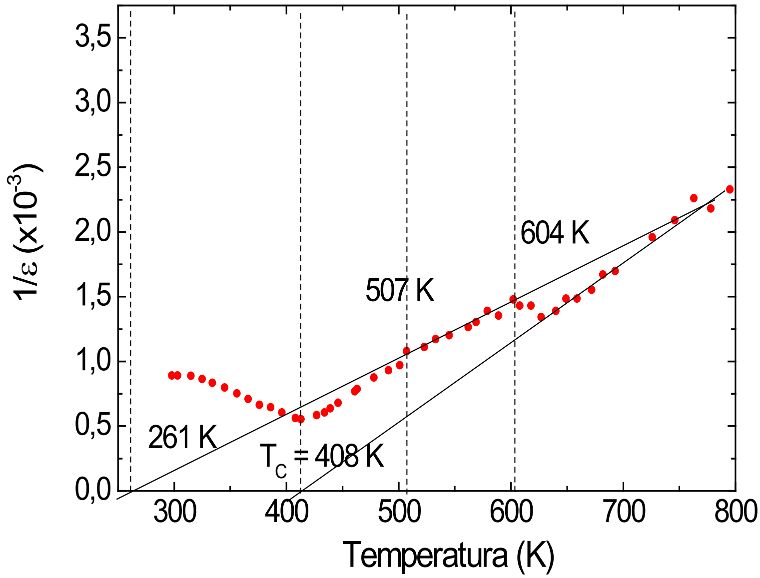

7 CONCLUSION

In the cryogenic temperature domain of the permittivity curve, the large area of hysteresis below Curie's temperature of relative maximum was associated to the intrinsic structural distortion with major contributing of niobium that exhibits distinct degree of off-centering character. Electrical phenomena of interface polarization are reviewed from microstructural, electrical and specific crystalline features. Frequency values of the interfaces showed that the $KSr_2Nb_5O_{15}$ nanostructured ceramic can be used as electroactive components in the low frequencies domain.

REFERENCES

ABRAHAMS, S., C.; JAMIESON, P., B.; BERNSTEIN, J., L.; Ferroelectric tungsten bronze-type crystal structures III – potassium lithium niobate $K_{(6-x-y)}$ $Li_{(4+x)}$ $Nb_{(10+y)}$ O_{30}, **Journal of Chemical Physics**,v. 54, p. 2355, 1971.

H. El A. Belghiti, A. Simon, P. Gravereau, A. Villesuzanne, M. Elaatmani and J. Ravez, *Sol. State Sci.*, 2002, **4**, 933.

CARVAJAL, J.R. An Introduction to the Program FullProff 2000, CEA/Saclay, France, 2008.

MATOS, J.; LANFREDI, S.; MONTAÑA, R.; NOBRE, M.A.L.; FERNÁNDEZ DE CÓRDOBA, M. C.; ANIA, C. O. Photochemical reactivity of apical oxygen in $KSr_2Nb_5O_{15}$ materials for environmental remediation under UV irradiation, **Journal of Colloid and Interface Science**, v. 496, p. 211–221, 2017.

LANFREDI, S.; DARIE, C.; BELLUCCI, F.S.; COLIN, C.V.; NOBRE, M.A.L. Phase transitions and interface phenomena in the cryogenic temperature domain of a niobate nanostructured ceramic, **Dalton Transaction**s, v. 43, p. 10983, 2014.

LANFREDI, S.; PALACIO, G.; BELLUCCI, F. S.; COLIN, C. V.; NOBRE, M. A. L. Thermistor Behavior and Electric Conduction Analysis of Ni-Doped Niobate Ferroelectric: the Role of Multiples β Parameters, **Journal of Physics D: Applied Physics**, v. 45, p. 435302, 2012.

LANFREDI, S.; BRITO, I.A.O.; POLINI, C.; NOBRE, M.A.L. Deriving the magnitude of niobium off-center displacement in ferroelectric niobates from infrared spectroscopy **Journal of Applied Spectroscopy**, v.79, p. 254-260, 2012.

LANFREDI, S.; CARDOSO, C.X.; NOBRE, M. A. L. Crystallographic properties of $KSr_2Nb_5O_{15}$, **Materials Science and Engineering B-Solid State Materials for Advanced Technology**, v. 112, p. 139-143, 2004.

LANFREDI, S.; LENTE, M. H.; EIRAS, J. A. Phase transition at low temperature in $NaNbO_3$ ceramic, **Applied Physics Letter,** v. 80, p. 2731-2733, 2002.

MAGNELI, A.; The crystal structure of tetragonal potassium tungsten bronze, **Ark. Kemi**, v. 24, p. 213, 1949.

NOBRE, M. A. L.; LANFREDI, S. Phase transition in sodium lithium niobate polycrystal: an overview based on impedance spectroscopy, **Journal of Physics and Chemistry of Solids***,* v. 62, p. 1999-2006, 2001.

NOBRE, M. A. L.; LANFREDI, S. Impedance Spectroscopy Analysis of High-Temperature Phase Transitions in Sodium Lithium Niobate Ceramics. **Journal of Physics: Condensed Matter**, v. 12**,** p.7833-7841, 2000.

PECHINI, M. P. "Method of Preparing Lead and Alkaline-Earth Titanates andNiobates and Coating Method Using the Same to Form a Capacitor," U.S. Pat. No. 3 330 697, July 11, 1967.

SHANMING, K. E.; HUIQING, F.; HUANG, H.; CHAN, H. L. W.; YU, S. Dielectric, ferroelectric properties, and grain growth of CaxBa1-xNb2O6 ceramics with tungsten bronzes structure. **Journal of Applied Physics**, v. 104, p. 24101, 2008.

TRIBOTTE, B.; HERVIEU, M.; DESGARDIN, G.; Dieletric and structural properties of A-cation-deficient perovskites, tetragonal tungsten bronzes and their composites in the $K_2Sr_4(Mg_xNb_{10-x})\ Li_{3x}O_{30}$ system, **Journal of Materials Science**, v. 33, p. 4609, 1998.

ABOUT THE ORGANIZER

MARCOS AUGUSTO DE LIMA NOBRE: Assistant Professor and Researcher (2006 - present), with citation name M. A. L. Nobre, at the São Paulo State University (UNESP), School of Science and Technology, Department of Physics, campus at Presidente Prudente-SP. Head and Founder (2002) of the Laboratory of Functional Composites and Ceramics (LaCCeF acronym in Portuguese, the native idiom), Lab certified by PROPE-UNESP/National Council for Scientific and Technological Development/CNPq*. Grants from National Council for Scientific and Technological Development (CNPq), 2020-2023, 2019-2021 and 2010-2012. Granted with Young-Researcher scholarship by the São Paulo Research Foundation, FAPESP (São Paulo, São Paulo) (2002 - Summer of 2005). Postdoctoral fellow at the Polytechnic School of the University of Sao Paulo (POLI USP-SP) Metallurgy and Materials Science Department with FAPESP Scholarship (1999-summer of 2000). PhD in Science, CAPES Scholarship (Physical Chemistry 1999) by the Chemistry Department, UFSCar-SP. Master in Chemistry CNPq scholarship (Physical Chemistry 1995) by the Chemistry Department, UFSCar-SP. Licentiate degree (4-year of study) in Physics (1993) CNPq and CNPq-Rhae scholarships by the Physics Department, UFSCar-SP. Associate Editor of the Micro & Nano Letters - IET 2019-2020. Associate Editor of the Micro & Nano Letters-Wiley, 2020 - present. Ethycal Editor of the Applied Mathematics Science (Reuse) m-Hikari and Modern Research in Catalysis, Irvine-CA, USA (2017- date). Editorial board member of the Artemis Editora, Brazil. Nowadays, have 02 patents. Has published 80 papers at 39 different indexed Journals of renowned Editors. In May/25/2021, has been cited 1379 times, at 76 papers (47 with citations), in according to the ResearchID actual Publons base having an H-index equal to 23. Academic Google score: H = 28, i10 = 45 and 2338 citations. Reviewer of more than three dozen of journals. Have more than 580 communications and presentation in National and International Congress and Symposiums, from these 150 has been published as Conference Paper. Author or co-author of 20 Chapters of book approaching Scientific Divulgation, Teaching of Physic and Chemistry for teachers actuating in the graduating degree. For this, the Nanoscience and Nanotechnology have been the first strategy. Received tens of National and International Awards, Honorable mentions and distinction mentions, as well as titles. Research skills: Materials Science, Advanced Ceramic Processing, Linear and Non-linear Advanced Dielectrics Materials, Solid state chemistry, Impedance spectroscopy of solids and fluids, Structural Characterization via Mid infrared Spectroscopy with Fast-Fourier-Transformed of solid and fluids, Structural and non-structural Phase Transitions in Semiconductor Ferroelectrics. Also, Molecular Interactions in Functional Fluids as biofuels and its blends, probed via mid infrared Spectroscopy. Research interests: New Functional Materials as amorphous composite based on carbon/nanoparticles and Semiconductor Ferroelectrics. Member of the Program of Post-Graduation in Chemistry at UNESP - Campus of São José do Rio Preto, IBILCE UNESP – SP, Brazil.

INDEX

A

B

C

D

E

F

P

R

S

U

V

X

Z

EDITORA
ARTEMIS